DAMAGE ASSESSMENT OF URBAN AREAS DUE TO THE 2015 NEPAL EARTHQUAKE USING PALSAR-2 IMAGERY

Rendy Bahri[1], Wen Liu [2] and Fumio Yamazaki [3]

Department of Urban Environment Systems, Chiba University
1-33 Yayoi-cho, Inage-ku, Chiba 263-8522, Japan;
[1] rendy.bahri@gmail.com; [2] wen.liu@chiba-u.jp; [3] fumio.yamazaki@faculty.chiba-u.jp

KEY WORDS: SAR backscatter, PALSAR-2, damage assessment, urban area, the 2015 Nepal earthquake

ABSTRACT: Damage assessment is an important issue in emergency response and recovery after nature disasters. In this regard, satellite remote sensing is recognized as an effective tool for detecting and monitoring affected areas. Since SAR sensors can capture images not only at daytime but also at nighttime and under cloud-cover, they are useful for damage mapping. In this study, we used multi-temporal high-resolution ALOS-2 PALSAR-2 images to detect the affected areas in Katmandu, which was severely affected by the April 25, 2015 Nepal (Gorkha) Earthquake. ALOS-2 images obtained before and after the earthquake were utilized for calculating the difference and correlation coefficient of the SAR backscatter. The affected areas were identified by high values of the difference and low values of the correlation coefficient. The pre- and post-event high-resolution optical satellite images were employed as ground truth data to verify the extraction results. Although it was difficult to estimate the damage levels of individual buildings, the high-resolution L-band SAR images could illustrate their capability in assessing damage situation in a city block level.

1. INTRODUCTION

The 2015 Nepal Earthquake with Mw 7.8 occurred at 11:56 (the local time, UTC 06:11) on 25 April and killed more than 8,800 people and injured more than 23,000 people. Its epicenter was in the east of Lamjung District, which is 80 km northwest of the capital city Kathmandu. The focal depth was approximately 15 km. A major aftershock of Mw 6.7 occurred on 26 April 2015 in the same region at 12:55 (the local time, UTC 07:10), with the epicenter located at about 17 km south of Kodari in Sindhupalchowk District, Nepal. Kathmandu is one of the severely affected cities due to the earthquake. Centuries-old buildings were destroyed at UNESCO World Heritage sites in the Kathmandu Valley, including some at the Kathmandu Durbar Square, the Patan Durbar Square, the Bhaktapur Durbar Square, the Changu Narayan Temple and the Swayambhunath Stupa. Kathmandu City is characterized by its high population density and vast manmade features in comparison to the surrounding areas. It means this urban area is the very important function place for the country. Hence it is very important to grasp the situation of the affected areas in the aftermath to take some proper actions.

Remote sensing is recognized as an effective tool for detecting and monitoring the affected areas after the occurrence of a natural disaster. Remote sensing is the science of acquiring, processing and interpreting images that record the interaction between the electromagnetic energy and materials (Sabins, 1996). Based on the sensor types, there are mainly two categories of remote sensing: the passive remote sensing (mainly optical sensors) and the active remote sensing (mainly radar sensors). Optical satellite system only works in the daytime and cannot observe objects under cloud-cover. However, a radar system as Synthetic Aperture Radar (SAR) overcomes this problem. Hence it is widely used in various emergency situations. SAR images have also been used in interferometric analysis to investigate damage to buildings (Ito et al., 2000; Yonezawa and Takeuchi, 2001). Comparing the changes in pre- and post-event SAR intensity images, damage detection of buildings has been conducted by several researchers (Matsuoka and Yamazaki, 2004; Dell'Acqua & Gamba, 2012). Recently, several studies attempted to detect damage at the scale of a single building unit, using both high-resolution optical and SAR images (Brunner et al., 2010; Uprety and Yamazaki, 2013).

Succeeding PALSAR onboard ALOS which terminated in April 2011, PALSAR-2 onboard ALOS-2 started its mission in May 2014. In this study, PALSAR-2 L-band SAR images obtained before and after the Nepal earthquake as an emergency-response support (Japan Aerospace Exploration Agency, 2015) are used to detect affected areas in Kathmandu City. The difference and correlation coefficient are calculated from the backscattering coefficient. The affected areas are identified by high values in the difference and low values in the correlation coefficient. The high-resolution optical satellite images are employed as ground truth data to verify the results from PALSAR-2 images.

2. THE STUDY AREA AND IMAGERY DATA USED

The study area of this paper is Kathmandu that is the capital city and the largest municipality in Nepal including the neighboring city Bhaktapur, as shown in **Figure 1**. This region is the only city in Nepal with the administrative status of Mahanagar (Metropolitan City), as compared to Upa-Mahanagar (Sub-Metropolitan City) or Nagar (City). Kathmandu is the core of Nepal's largest urban agglomeration, located in the Kathmandu Valley consisting of Lalitpur, Kirtipur, Madhyapur Thimi, Bhaktapur and a number of smaller communities.

The data employed in this research were taken by ALOS-2 satellite system operated by JAXA (Japan Aerospace Exploration Agency). ALOS-2 was launched on May 24, 2014, with an enhanced SAR sensor PALSAR-2. The pre-event image was captured on February 21, 2015 (two months before the earthquake) and the post-event image was captured on May 2, 2015 (one week after the earthquake). The acquisition mode of the both images was StripMap, with HH and HV polarizations and an incidence angle of 36.29 degrees at the center of the images. The satellite path was ascending with right-looking. The resolution was 7.2 m in the azimuth direction and 4.3 m in the slant-range direction.

The images were provided as the range and single-look azimuth compressed data with the processing level 1.1, which were represented by the complex I and Q channels to preserve the amplitude and phase information. After several pre-processing steps using *ENVI/SARscape* software, these images were projected to the WGS84 reference ellipsoid with a pixel spacing of 5 m. Radiometric calibration of each intensity image was carried out to get the backscattering coefficient (sigma naught, σ^0) in the ground range in the decibel (dB) unit, represented by the following equation.

$$\sigma^0(\text{dB}) = 10\log_{10}(DN^2) + CF \quad (1)$$

where σ^0 means the backscattering coefficient per unit area in the ground range, and DN is the digital number of a pixel; *CF* is the calibration factor, which is -83 dB. After this conversion, an adaptive filter (Lee, 1980) was applied to the original SAR images to reduce the speckle noise, which makes the radiometric and textural aspects less efficient, and to improve the correlation coefficient between the two images.

Figure 2 shows the color composite of the pre- and post-event images for the HH and HV polarizations. We tried to compare the result for the two polarizations, and it was found that the HH polarization shows a better result than the HV polarization does. Thus in this study, we use the HH polarization to assess the situation of an urban area due to the 2015 Nepal Earthquake. The target area was extracted at the center of Kathmandu and enlarged as shown in **Figure 3**, including Durbar Square, Tundikhel and Dharahara Tower. A color composite of the pre- and post-event SAR images is also shown in the figure, in which several changed areas could be confirmed by red (increased) and

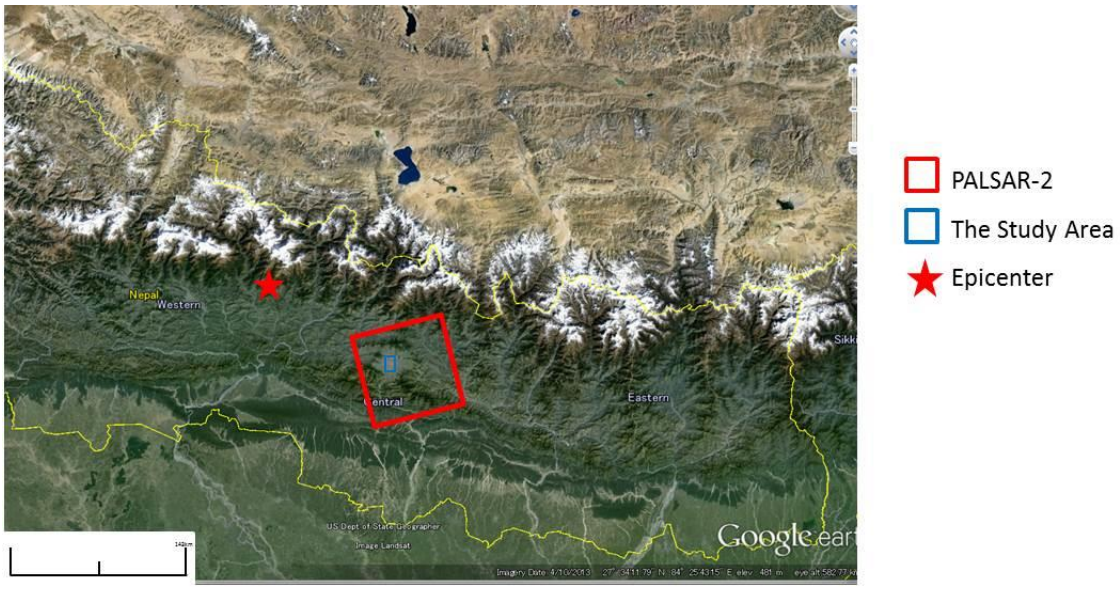

Figure 1. Location of the study area in the central Nepal.

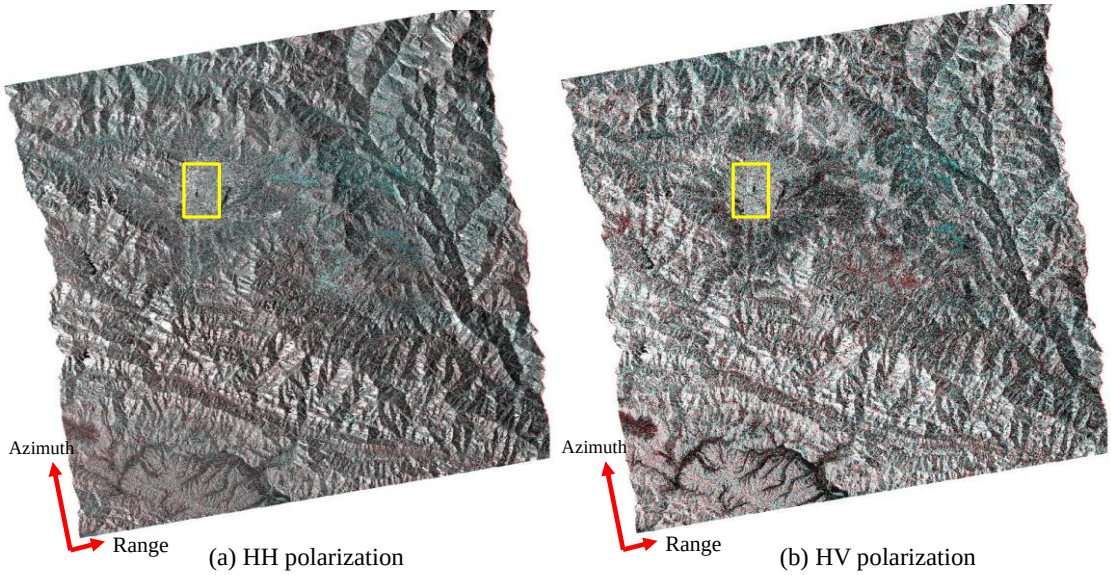

(a) HH polarization (b) HV polarization

Figure 2. Color composite of HH (a) and HV (b) polarizations, where the Kathmandu area is shown in the yellow frame.

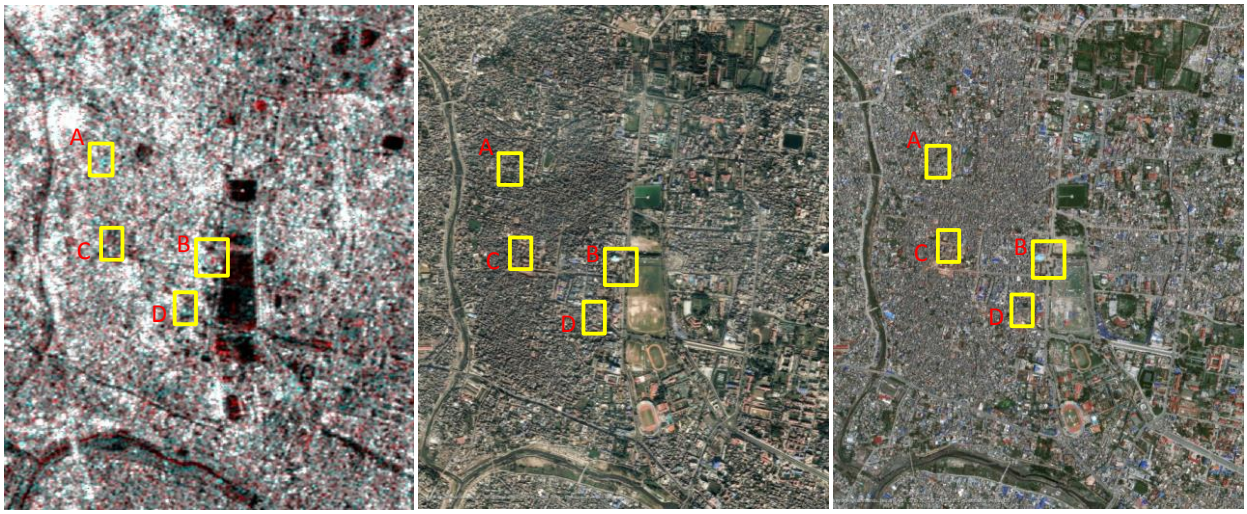

(a) Color Composite (b) Pre-event Optical Images (c) Post-event Optical Images

Figure 3. Close-up of the central Kathmandu: (a) a color composite of the PALSAR-2 images with the post-event one in the red band and the pre-event one in the blue and green bands (cyan); (b) the pre-event optical image (November 29,2014); (c) the post-event optical image (April 27,2015) taken by Pleiades satellite.

cyan (decreased backscatter after the earthquake) colors. The grey areas represent the unchanged areas over the time. Four yellow squares show the areas that will be discussed in detail in this study. A pre-event optical satellite image taken by Pleiades (Airbus Defence and Space, 2015) on November 29, 2014 (**Figure 3(b)**) and a post-event one taken also by Pleiades on April 27, 2015 (**Figure 3(c)**) were introduced to verify our results from the PALSAR-2 data. Pleiades is the constellation operated by CNES for the earth observation mission, launched on December 17, 2011 (Pleiades 1A) and on December 2, 2012 (Pleiades1B).

3. DAMAGE DETECTION AND THE RESULTS

The change detection from two-temporal SAR intensity images can be evaluated quantitatively by their backscattering difference value (*d*) and the correlation coefficient (*r*), calculated from Equations (2) and (3). The window size was set first as from 3×3 pixels to 21×21 pixels. According to the visual comparison of the results, the 5×5 pixels window was adopted to obtain *d* and *r* in this study.

$$d = \bar{I}a_i - \bar{I}b_i \tag{2}$$

$$r = \frac{N\sum_{i=1}^{N} Ia_i Ib_i - \sum_{i=1}^{N} Ia_i \sum_{i=1}^{N} Ib_i}{\sqrt{(N\sum_{i=1}^{N} Ia_i^2 - (\sum_{i=1}^{N} Ia_i)^2)\cdot (N\sum_{i=1}^{N} Ib_i^2 - (\sum_{i=1}^{N} Ib_i)^2)}} \tag{3}$$

where Ia_i, Ib_i represent the *i*-th pixel vales of the post- and pre-event SAR backscattering coefficient values, respectively, and $\bar{I}a_i$and $\bar{I}b_i$ are the average values of the 7×7 pixels surrounding the *i*-th pixel. The correlation coefficient (*r*) is a scalar quantity between -1.0 and 1.0, and used to find the measure of correspondence between two-sample populations. A high positive value of *r* indicates no change between the pre- and post-event images whereas a low value indicates the strong possibility of change (Brown, 1992).

Figure 4 shows the difference of the backscattering coefficients (*d*), ranging from -11 dB to 11 dB, and the correlation coefficient (*r*), ranging from -0.9 to 0.9, between the pre- and the post-event images. In this study, we used a 5×5 pixels window (25 m × 25 m) to calculate these values. We selected four study areas from the central Kathmandu in order to explain the tendency to discriminate damaged and non-damaged areas using the difference and the correlation coefficient of the two-temporal sigma naught values.

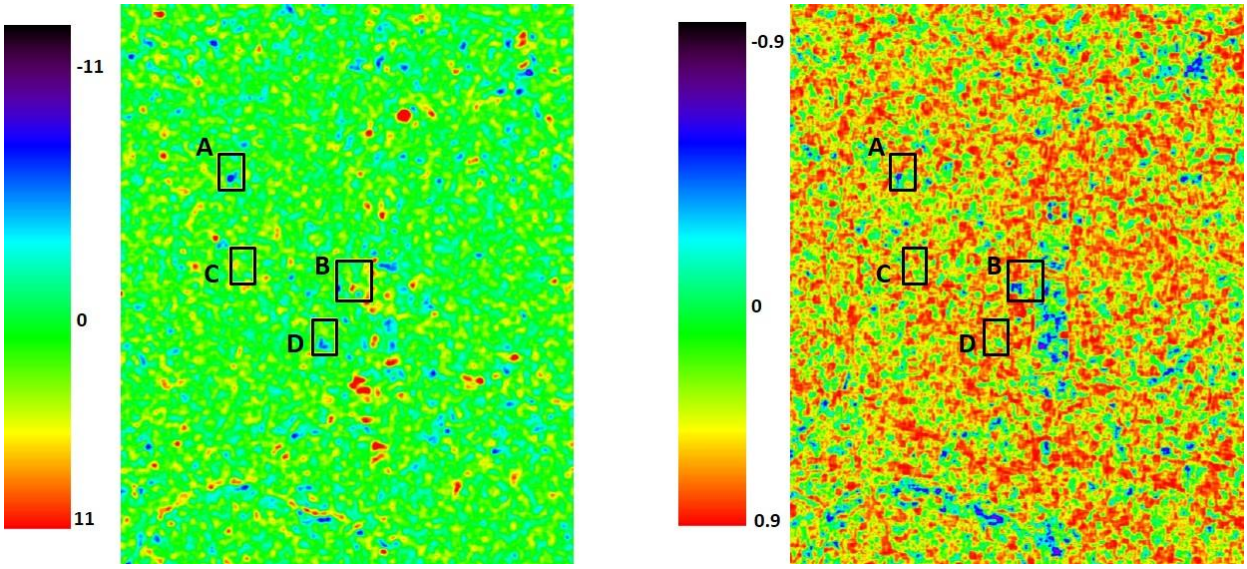

(a) Difference (b) Correlation coefficient

Figure 4 (a) Difference and (b) correlation coefficient for the central Kathmandu obtained from the pre- and post-event PALSAR-2 images

3.1. Study Area A

Figure 5 shows an enlarged plot for the study area A (**Figure 3**) in the central Kathmandu. Changed areas are shown in two red squares and unchanged areas shown in three white squares in the figure. The difference of the pre- and post-event σ^0 values show different trends at the two changed blocks. In the block **b**, decreased (negative in *d*) values are dominant within the 5×5 pixel window while increased (positive in *d*) values are dominant in the block **a**. Low correlation coefficient values (less than 0.5 to negative values) are observed for the both blocks, indicating changes. On the contrary, the three unchanged blocks (corresponding to large buildings) shows high correlation values and small differences, representing no big change between the two acquisition times. The pre- and post-event Pleiades images, shown in **Figure 5 (d, e)**, explain these observed situations.

The blocks ***a*** and ***b*** are further enlarged in **Figure 6** in order to observe more details of damaged buildings. In the block ***a***, the increased backscatter was seen although a large building was collapsed in it. We confirmed that the roof of the collapsed building was flat, showing small backscatter before the earthquake. After the earthquake, the rubble of the collapsed building reflected the microwave stronger than before, that made the difference increased. In the block ***b***, a large building with a gable roof showing strong microwave reflection existed before the event. Due to the earthquake, the building collapsed completely that made the SAR backscatter smaller than before. The enlarged images for the block ***l*** are also shown in the figure and no significant change is observed.

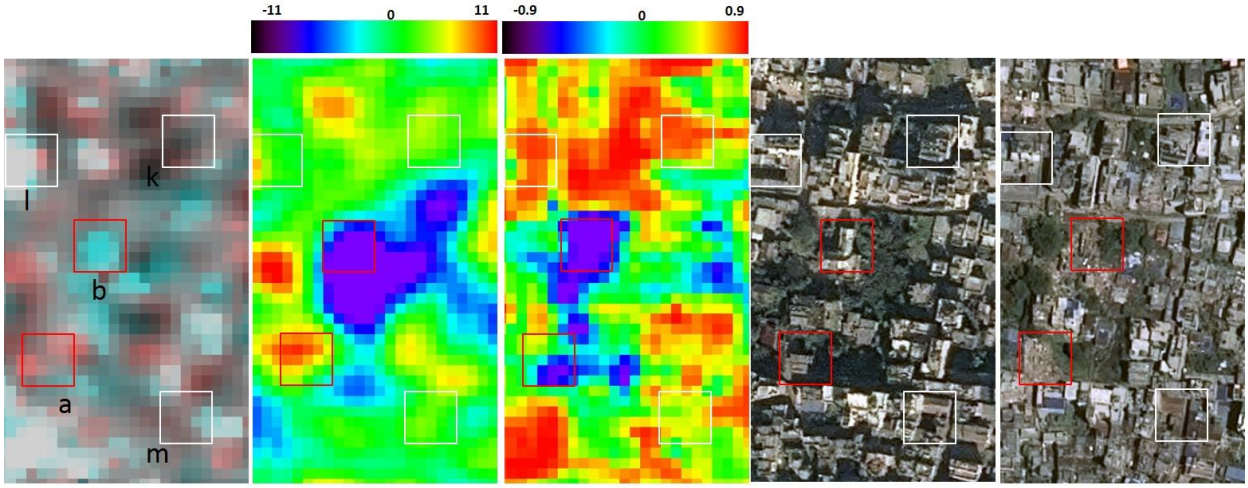

(a) Color composite (b) Difference (c) Correlation coefficient (d) the pre-event image (e) the post-event image

Figure 5. Close-up of the area A: (a) the color composite of the calibrated SAR images, (b) difference, (c) correlation coefficient,(d) the pre-event Pleiades image, (e) the post-event Pleiades image.

(a) The block ***a*** (b) The block ***b*** (c) The block ***l***

Figure 6. Close-up of the enlarged optical images for the blocks ***a*** (a), ***b*** (b) and ***l*** (c) (left: pre-event, right: post-event).

3.2 Study Area B

Figure 7 shows an enlarged plot for the study area B (**Figure 3**) including a large green named Tundikhel. After the earthquake, a lot of citizens evacuated to Tundikhel and it became like tent villages. Changed areas were selected and are shown in two red squares, and unchanged areas shown in three white squares in the figure. Different trends are also observed in the difference of the pre- and post-event σ^0 values at the two changed blocks. In the block ***c***, decreased values are dominant within the 5×5 pixel window while increased values are dominant in the block ***d***. Low correlation coefficient values indicating changes are observed for the both blocks. The three unchanged blocks corresponding to large buildings, ***n*** and ***p*** (Kathmandu Mall), many small buildings (***o***) shows high correlation values and small differences. These observations can be explained by the pre- and post-event optical images.

In order to observe more details of damaged buildings, the blocks ***c***, ***d***, ***p*** are further enlarged in **Figure 8**. In the block ***c***, two large buildings (Military Hospital) existed before the event as seen by their shadows, but they disappeared after the earthquake. These buildings might be collapsed and then demolished or removed before the earthquake for other reasons. This change made the SAR backscatter smaller than before. In the block ***d*** (Tundikhel), the tents of refugees were placed after the earthquake as described before, showing stronger backscatter than the empty ground in the pre-event time. Kathmandu Mall in the block ***p*** shows no apparent change between the pre- and post-event optical images.

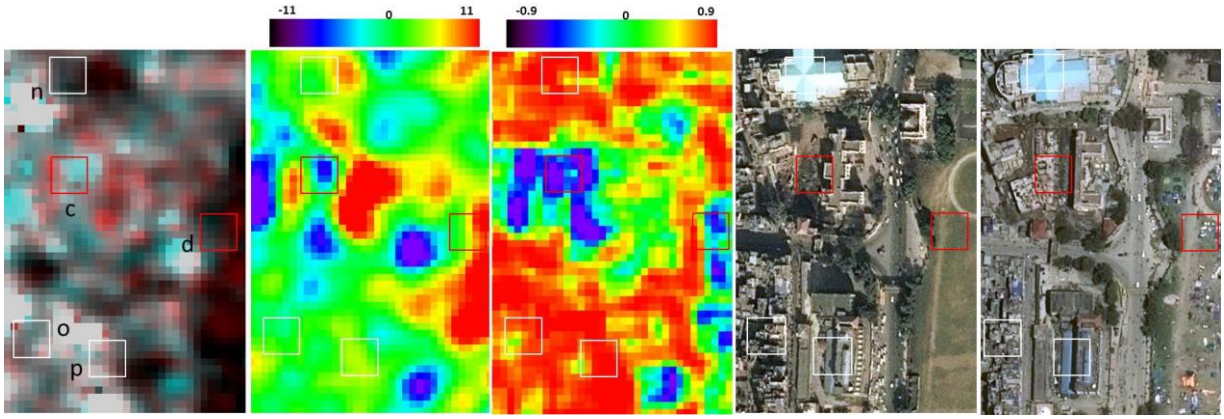

(a) Color composite (b) Difference (c) Correlation coefficient (d) the pre-event image (e) the post-event image

Figure 7. Close-up of the area B: (a) the color composite of the calibrated SAR images, (b) difference, (c) correlation coefficient,(d) the pre-event Pleiades image, (e) the post-event Pleiades image.

(a) The block ***c*** (b) The block ***d*** (Tundikhel green) (c) The block ***p*** (Kathmandu Mall)

Figure 8. Close-up of the enlarged optical images for the blocks ***c*** (a), ***d*** (b) and ***p*** (c) (left: pre-event, right: post-event).

3.3 Study Area C

An enlarged plot for the study area C including the Durbar Square, one of the World Heritage sites in Kathmandu, is shown in **Figure 9**. Changed areas were selected from the optical images and are shown in two red squares and unchanged areas in three white squares in the figure. In the block ***e*** including Kasthamandap Hindu temple, the backscatter difference did not change so much and the correlation was moderately low although this structure was completely collapsed as shown in **Figure 10**. On the contrary, the block ***f*** including Maju Deval, the difference value was negative and the correlation was not so high. This observation is consistent with the damage status (collapse) of this tower.

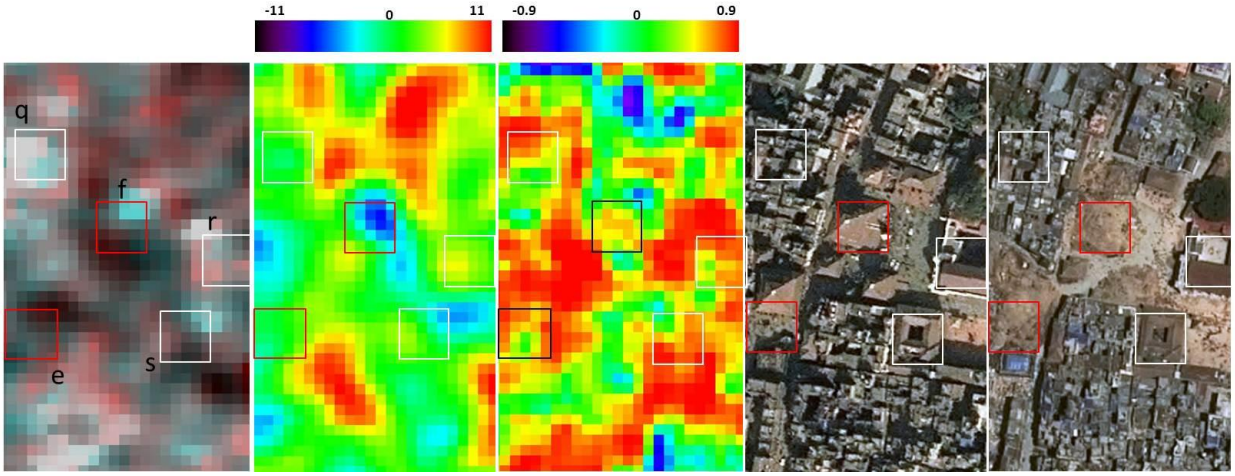

(a) Color composite (b) Difference (c) Correlation coefficient (d) the pre-event image (e) the post-event image

Figure 9. Close-up of the area C: (a) the color composite of the calibrated SAR images, (b) difference, (c) correlation coefficient,(d) the pre-event Pleiades image, (e) the post-event Pleiades image.

Figure 10. Snapshot of aerial video taken from UAV (https://www.youtube.com/watch?v=N52LX1GZYWs) over the Durbar Square including the blocks ***e*** (Kasthamandap) and ***f*** (Maju Deval).

For the three unchanged blocks (corresponding to a large building: ***r*** and ***s***, many small buildings: ***q***), the difference was seen to be no much change and the correlation coefficient was generally high.

3.4 Study Area D

Figure 11 shows an enlarged plot for the study area D including Bhimsen Tower (or Dharahara). The nine-story tower of 61.9 m tall was collapsed and many people were killed. Changed areas were selected as shown in two red squares (***g*** and ***h***) and unchanged areas shown in two white squares in the figure. Different trends are also observed in the difference of the pre- and post-event σ^0 values at the two changed blocks. In the block ***g***, decreased values are dominant within the 5×5 pixel window and slightly decreased values are observed in the block ***h*** including Bhimsen Tower's base. The correlation coefficient values for these two blocks are moderately high to low, indicating some changes are observed for the both blocks. In the block ***h***, Bhimsen Tower in the middle collapsed but the diameter of the tower was not so large, and hence the reduction of backscatter due to this damage was not so high. The reduction in the block ***g*** might be caused by the collapse of buildings in the west side, not by the tower collapse. The two unchanged blocks, ***u*** and ***t***, show high correlation values and small differences as expected from the pre- and post-event optical images. A snapshot of drone video footage of the area D is shown in **Figure 12**. The damage situation of the area is more easily observed from the oblique shot.

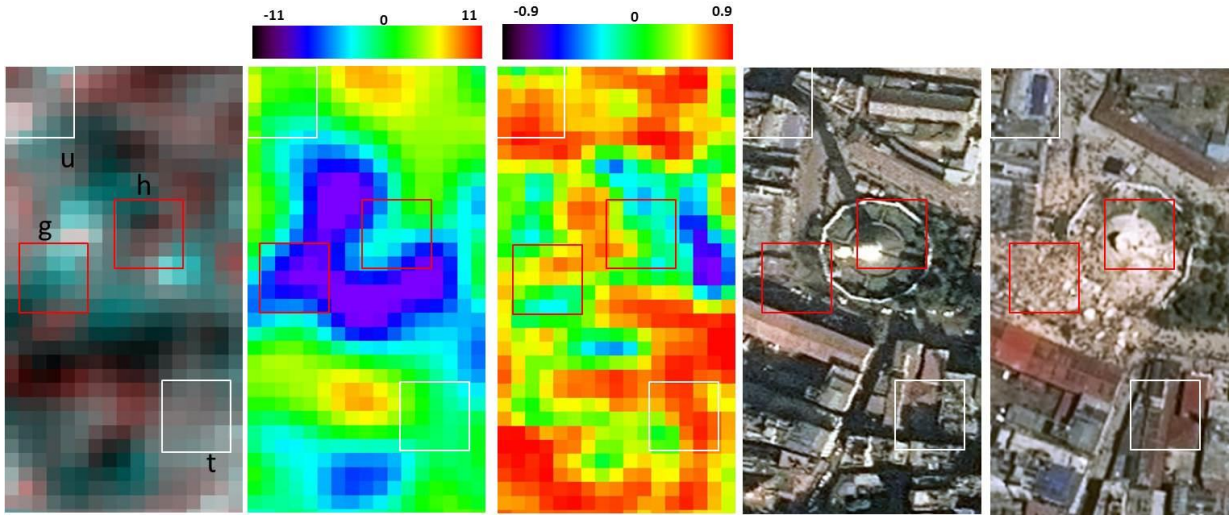

Figure 11. Close-up of the area D: (a) color composite of the calibrated SAR images, (b) difference, (c) correlation coefficient, (d) the pre-event Pleiades image, (e) the post-event Pleiades image.

Figure 12. Snapshot of aerial video taken from UAV (https://www.youtube.com/watch?v=KtXv7PLnR4o) over the Bhimsen Tower area including the blocks ***g*** and ***h***.

4. DISCUSSION ON CLASSIFYING DAMAGED AND NON-DAMAGED BLOCKS

As described above, we examined the change in the difference and the correlation coefficient between the two time-instants for 8 damaged and 11 non-damaged blocks. In this study, these indices were calculated for the whole imaging area using 5×5 pixels window. This means the central pixel of a 25 m × 25 m window represents the values within the window. The relationship of these two indices for the 19 blocks is shown in **Figure 13**. In the figure, non-changed blocks are characterized by correlation coefficient values higher than 0.46 while damage blocks lower than 0.43. The classification of damage and non-damage is also possible using the difference. All the non-damaged blocks falls in the range -2.0 dB to 2.0 dB while the damaged blocks are outside of this range except for the block ***e***. These threshold lines highly depend on the data selection, and hence we must select more blocks even in Kathmandu and, of course, in other cities in Nepal.

But as tentative thresholds, these two criteria were used to extract the pixels including possible changes between the two time-instants. **Figure 14** shows the part of the city including the four study areas and the extracted result of changed pixels in yellow color. The changed pixels were determined as the correlation coefficient smaller than 0.45 and the difference smaller than -2.0 dB or larger than 2.0 dB, as shown in the two ranges in **Figure 13**. By these thresholds, the selected changed locations look reasonably well although more detailed examination is necessary.

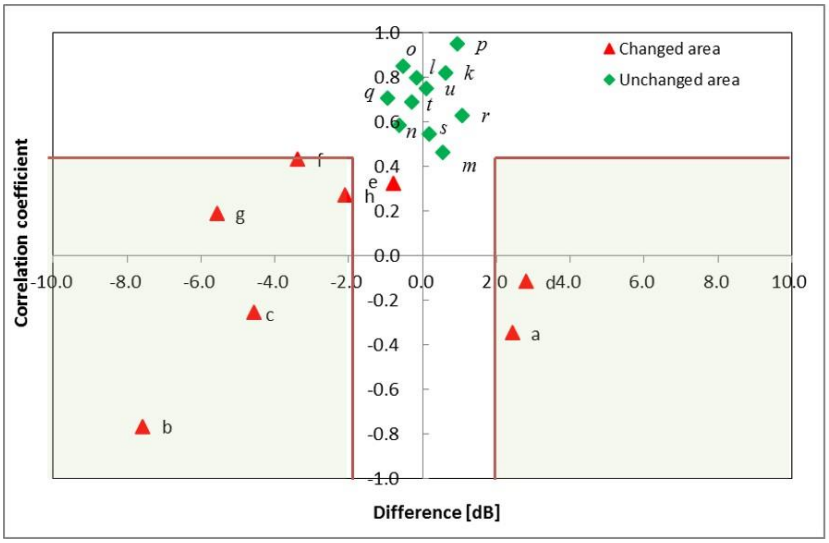

Damage Status	Block ID	Difference [dB]	Correlation Coefficient
Damaged	a	2.430	-0.347
	b	-7.587	-0.767
	c	-4.558	-0.253
	d	2.794	-0.116
	e	-0.788	0.325
	f	-3.387	0.432
	g	-5.577	0.189
	h	-2.107	0.271
Non-Damaged	k	0.619	0.818
	l	-0.162	0.797
	m	0.546	0.462
	n	-0.631	0.586
	o	-0.527	0.852
	p	0.947	0.951
	q	-0.945	0.709
	r	1.079	0.629
	s	0.186	0.548
	t	-0.302	0.690
	u	0.096	0.751

Figure 13 Scatter plot of the difference and the correlation coefficient of the pre- and post-event backscatter for 8 damaged and 11 non-damaged blocks in the study areas (A-D).

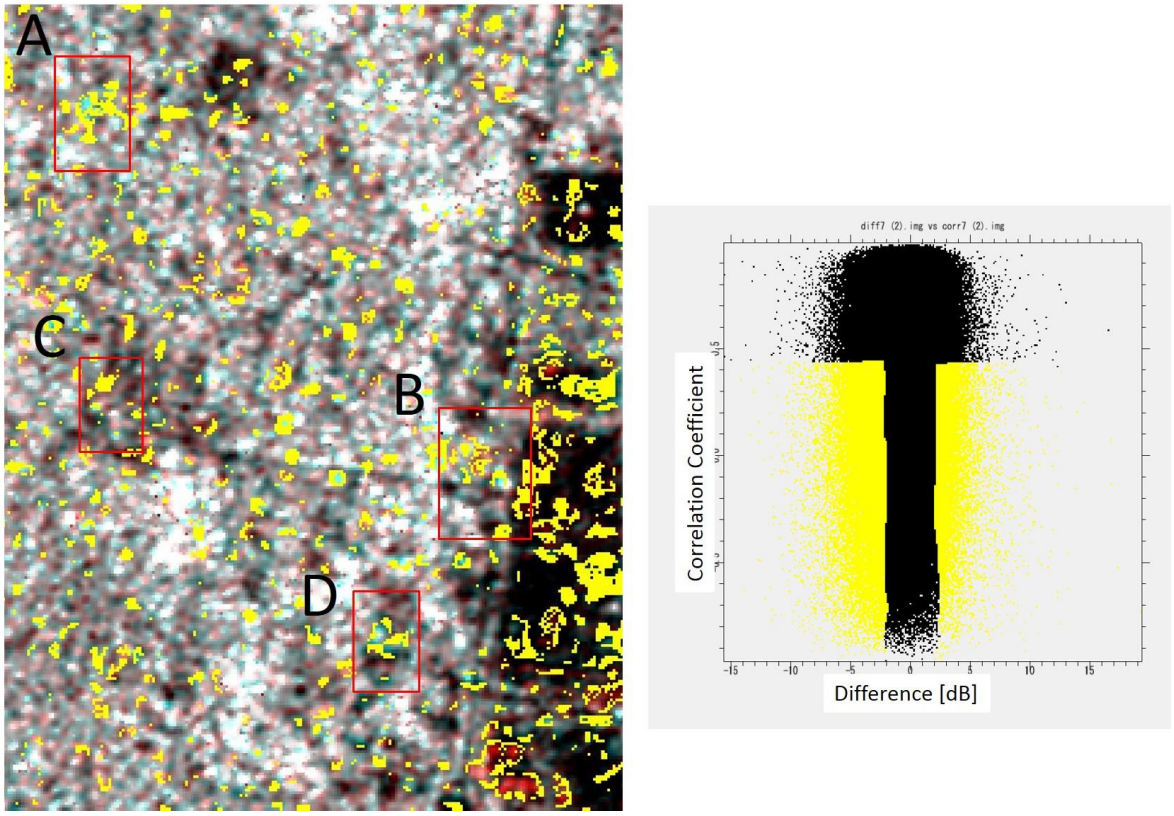

Figure 14 The part of the Kathmandu City including the four study areas (A-D) and the extracted changed pixels in yellow color. The damaged pixels were determined as the correlation coefficient smaller than 0.45 and the difference smaller than -2.0 dB or larger than 2.0 dB.

5. CONCLUSIONS

Using the ALOS-2 PALSAR-2 images acquired before and after the 2015 Nepal earthquake, the extraction of building damage was carried out for the central part of Kathmandu. The affected areas were estimated with the aid of the multi-temporal color-composite image, the difference and the correlation coefficient of the backscattering coefficient values at the two time-instants. Eight city blocks (25 m × 25 m) including damaged buildings/towers and eleven blocks without apparent damage were selected. By this examination, the affected blocks were mostly identified by high values of the difference and low values of the correlation coefficient. Pre- and post-event optical satellite images as well as drone footages were employed to assess the accuracy of the damage extraction from the L-band SAR imagery. By setting threshold values for the two indices obtained from the SAR data, the overall distribution of building damage in a city block level was realized. Although this study is still preliminary, we highlighted the capability of PALSAR-2 imagery in extraction of building damage in dense urban areas. A further research will be carried out using more imagery data from PALSAR-2 to validate their usefulness in emergency response activities.

ACKNOWLEDGMENT

The ALOS PALSAR-2 data used in this study are owned by Japan Aerospace Exploration Agency (JAXA), and were provided through the JAXA's ALOS-2 research program (RA4, PI No. 1503). The Pleiades images are owned by Airbus Defence and Space and the pre- and post-event JPG files used in this study were downloaded from the company's web site.

REFERENCES

Airbus Defence and Space, 2015. Kathmandu, viewed by Pléiades satellites, before and after the earthquake, Retrieved May 1, 2015 from http://airbusdefenceandspace.com/newsroom/news-and-features/kathmandu-viewed-by-pleiades-satellites-before-and-after-the-earthquake/

Brown, L.G., 1992. A survey of image registration techniques. ACM Computing Surveys, 24 (4).

Brunner D., Lemoine G. and Bruzzone L., 2010. Earthquake damage assessment of buildings using VHR optical and SAR imagery. IEEE Transactions on Geoscience and Remote Sensing, 48(5), pp. 2403–2420.

Dell'Acqua, F., & Gamba, P. 2012. Remote sensing and earthquake damage assessment experiences, limits, and perspectives, Proceedings of the IEEE, 100,pp. 2876–2890.

Ito, Y., Hosokawa, M., Lee, H., and Liu, J.G., 2000. Extraction of damaged regions using SAR data and neural networks. International Archives s of Photogrammetry and Remote Sensing 2000, XXXIII, pp.156–163

Japan Aerospace Exploration Agency (JAXA), 2015. ALOS-2/PALSAR-2 observation results of the 2015 Nepal Earthquake (1), Retrieved May 1, 2015 from http://www.eorc.jaxa.jp/ALOS-2/en/img_up/dis_pal2_npl-eq_20150426.htm

Lee, J.S., 1980. Digital image enhancement and noise filtering by use of local statistics. IEEE Transaction on Pattern Analysis and Machine Intelligence, 2(2), pp.165-168.

Matsuoka, M., and Yamazaki, F., 2004. Use of satellite SAR intensity imagery for detecting building areas damaged due to earthquakes. Earthquake Spectra 2004, 20(3), pp. 975-994.

Sabins, F.F., 1996. Remote Sensing: Principles and Interpretation, Freeman, New York.

Uprety, P., and Yamazaki, F., Dell' Acqua, F., 2013. Damage detection using high-resolution SAR imagery in the 2009 L'Aquila, Italy, Earthquake. Earthquake Spectra, Vol. 29, No. 4, pp.1521-1535.

Yonezawa, C., and Takeuchi, S. (2001). Decorrelation of SAR data by urban damages caused by the 1995 Hyogoken-Nanbu Earthquake, International Journal of Remote Sensing, 22:8, pp.1585–1600.